molecules

MDPI

Article

Synthesis, Cyclooxygenases Inhibition Activities and Interactions with BSA of *N*-substituted 1*H*-pyrrolo[3,4-c]pyridine-1,3(2*H*)-diones Derivatives

Edward Krzyżak [1,*], Dominika Szkatuła [2], Benita Wiatrak [3], Tomasz Gębarowski [3] and Aleksandra Marciniak [1]

1 Department of Inorganic Chemistry, Wroclaw Medical University, ul. Borowska 211a, 50–556 Wrocław, Poland; aleksandra.marciniak@umed.wroc.pl
2 Department of Medicinal Chemistry, Wroclaw Medical University, Borowska 211, 50–556 Wroclaw, Poland; dominika.szkatula@umed.wroc.pl
3 Department of Basic Medical Sciences, Wroclaw Medical University, Borowska 211, 50–556 Wroclaw, Poland; benita.wiatrak@umed.wroc.pl (B.W.); tomasz.gebarowski@umed.wroc.pl (T.G.)
* Correspondence: edward.krzyzak@umed.wroc.pl; Tel.: +48-71-784-0330; Fax: +48-71-784-0336

Received: 9 June 2020; Accepted: 23 June 2020; Published: 25 June 2020

Abstract: Inhibition of cyclooxygenase is the way of therapeutic activities for anti-inflammatory pharmaceuticals. Serum albumins are the major soluble protein able to bind and transport a variety of exogenous and endogenous ligands, including hydrophobic pharmaceuticals. In this study, a novel *N*-substituted 1*H*-pyrrolo[3–c]pyridine-1,3(2*H*)-diones derivatives were synthesized and biologically evaluated for their inhibitory activity against cyclooxygenases and interactions with BSA. In vitro, COX-1 and COX-2 inhibition assays were performed. Interaction with BSA was studied by fluorescence spectroscopy and circular dichroism measurement. The molecular docking study was conducted to understand the binding interaction of compounds in the active site of cyclooxygenases and BSA. The result of the COX-1 and COX-2 inhibitory studies revealed that all the compounds potentially inhibited COX-1 and COX-2. The IC_{50} value was found similar to meloxicam. The intrinsic fluorescence of BSA was quenched by tested compounds due to the formation of A/E–BSA complex. The results of the experiment and molecular docking confirmed the main interaction forces between studied compounds and BSA were hydrogen bonding and van der Waals force.

Keywords: pyrrolo-pyridine derivatives; cyclooxygenase; anti-inflammatory; serum albumin interactions; fluorescence quenching; molecular docking

1. Introduction

Derivatives of 3,4-pyridinedicarboximides have been interesting for many years. Most of them show various kinds of biological activities. For example, *N*-(2,6-dimethylphenyl)-3,4- pyridinedicarboximide is active against MES (Maximal Electroshock Seizures) and appears to be a promising compound for the design of anticonvulsant drugs [1]. Some of [pyrrolo[3,4-c]pyridin-1,3(2*H*)-dion-2-yl] acetic acids derivatives show significant AR (aldose reductase) inhibitory activity [2]. The 3,4-pyridinedicarboximide was a base compound in the design and synthesis of azaisoindolinone derivatives with a lipophilic chain. These compounds were designed as InhA inhibitors and as anti-mycobacterium tuberculosis agents [3]. The derivatives of bicyclic hydroxy-1*H*-pyrrolopyridine-triones were designed as a new family of HIV-1 integrase inhibitors [4].

Cyclooxygenase (COX) is the key enzyme required for the conversion of arachidonic acid to prostaglandins. At least two isoforms of COX are known—COX-1 and COX-2. COX-1 is involved in the synthesis of prostaglandins responsible for maintaining normal body function in the kidney,

GIT, and other organs. COX-2 is the isoform that plays a major part in the inflammatory process and the pain associated with it [5,6]. COX-1 and COX-2 are the therapeutic targets for drugs, including ibuprofen, naproxen, diclofenac, or piroxicam, as well as newer COX-2 selective inhibitors. Through their anti-inflammatory, anti-pyretic, and analgesic activities, they represent a choice treatment in various inflammatory diseases such as arthritis, rheumatisms as well as relieving the pains of everyday life [7,8].

From a biopharmaceutical point of view, one of the most important biological functions of albumins is their ability to carry drugs. The drug-BSA (bovine serum albumin) or HSA (human serum albumin) interaction may result in the formation of a stable complex, which has a great impact on discovering pharmacokinetic and pharmacodynamics implications. Spectroscopic methods like fluorescence, UV-vis, and circular dichroism spectroscopies help acquire this knowledge.

A 2-[2-hydroxy-3-(4-aryl-1-piperazinyl)propyl] derivatives of 4-methoxy- and 4-ethoxy-6-methyl-1*H*-pyrrolo[3,4-c]pyridine-1,3(2*H*)-diones indicate strong analgesic properties (stronger than ASA and Morphine in writhing syndrome test), and they are non-toxic [9]. The compounds **A**–**C** presented in this work were designed by some modifications: shortening the chain between imide nitrogen and nitrogen of piperazine ring, elimination of the carboxyl group, and movement of the methyl group to 5 position (Figure 1). The compounds **D** and **E** are smaller and do not have a phenylo-piperazino ring. The compound A was previously synthesized and tested for anxiolytic effects [10]. However, no activity was found, only the potential analgesic effect was suggested. The aim of this work was the investigation of the synthesized compounds for their potencies to inhibit COX-1 and COX-2 enzymes and study the interaction with bovine serum albumin.

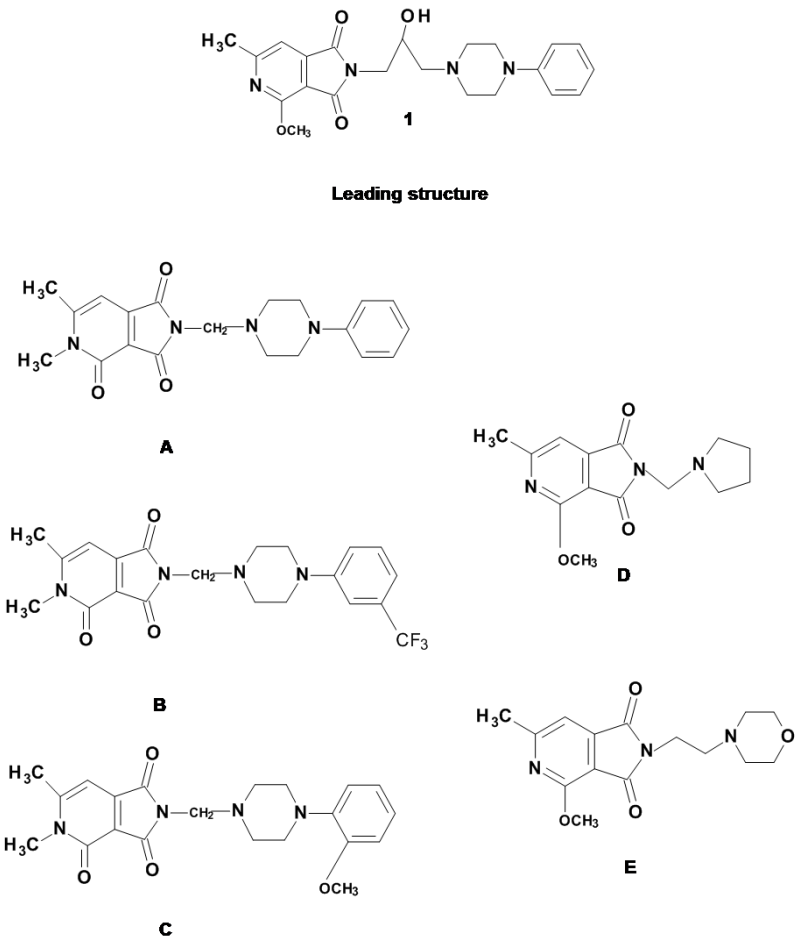

Figure 1. Lead and investigated compounds (**A**–**E**) of this study.

2. Results and Discussion

2.1. Chemistry

Synthetic scheme of the studied compounds, as shown in Scheme 1. The compounds **2**, **3** and **A** were obtained according to the literature data [10–13]. Imide **2** is the starting product for derivatives **A**, **B** and **C** and many other substances described earlier [10,14,15]. Compounds **2** and **3** differ slightly in structure, imide 3 contains a methoxy substituent attached to the carbon atom in a position adjacent to the nitrogen atom of the pyridine ring, while derivative **2** is its *N*-methylanalogue. To compare the biological properties of both basic systems, it was decided to synthesize analogues of the previously described derivatives containing the same amino residues: 1-phenylpiperazine (**A**), 1-(2-methoxyphenyl)piperazine (**B**) and 1-(3-trifluoromethyphenyl)piperazine (**C**) [9]. The presence of an acidic proton atom at the imide nitrogen atom in position 2 makes it possible to carry out the aminomethylation reaction according to the mechanism described by Mannich [13,16]. The reaction was carried out using aqueous solution of formaldehyde (HCHO) and N-arylpiperazines (commercial products Sigma-Aldrich) at the reflux temperature of tetrahydrofuran (THF) for several hours (method I, Scheme 1). The course of condensation was monitored by TLC. During the reaction of (**A** and **B**) or after the evaporation of the solvent (**C**) final products were obtained. Poor solubility in organic solvents (chloroform, ethanol, methanol, ethyl acetate) and their mixtures prevented the purification of the products by column chromatography, therefore the final compounds were tested in the form of crude products. NMR spectral analysis was performed in dimethyl sulfoxide (DMSO). All reactions proceeded with a very good yield of 79.4–93.8%.

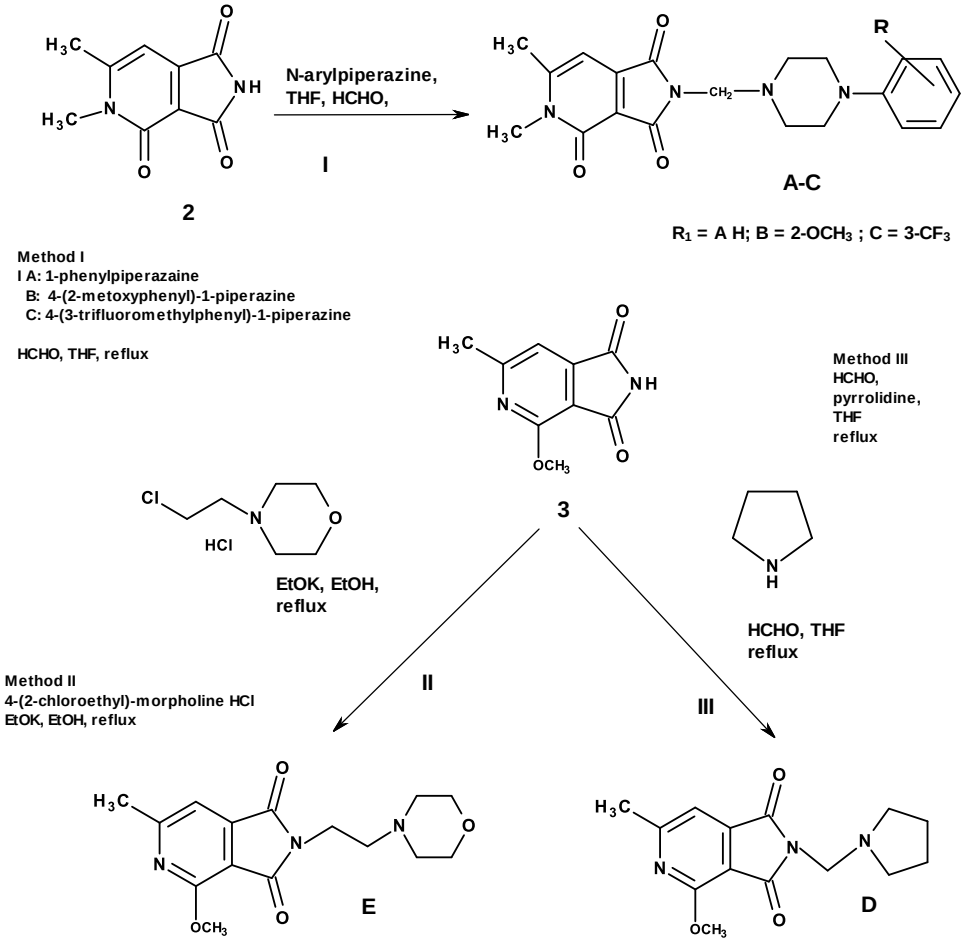

Scheme 1. Synthetic scheme of the studied compounds.

Imid **3**, previously described [11,13] was the starting product for the synthesis of several dozen derivatives with confirmed biological activity (Śladowska et al.) [9,13,17,18].

The main line of analogues was based on the structure of 4-alkoxy-1*H*-pyrrolo(3,4-c) pyridine-1,3(2*H*) -dione. Optimal biological properties in the behavioral tests showed imide**1**: 4-alkoxy-*N*- [3- (*N*-phenyl-4-piperazinyl) -2-hydroxy] propyl-1*H*-pyrrolo (3,4-c) pyridine-1, 3(2*H*)-dione. One of the structure modifications is the assumption of shortening to two (**E**) or one (**D**) methylene groups of the alkyl linker between the 2-methoxy-3,4-pyridinedicarbox imide moiety and the arylamine residue. In order to obtain **D** and **E** derivatives, commercial preparations of 4-(2-chloroethyl)-morpholine and pyrrolidine were used, condensing the potassium salt of imide **3**, under the influence of potassium ethoxylate in anhydrous ethanol (method II, Scheme 1; **E**), or in the Mannich reaction-THF-solvent and formalin (method III, Scheme 1; **D**). The reaction yield was 50% (**E**) and 60% (**D**).

2.2. Viability of Cell Cultures

MTT assay showed the concentration-dependence of cytotoxicity of tested compounds, and cell viability decreased with increasing concentration (Figure 2). After incubation with compounds **A**–**D** at 10 μM and **A** and **D** at 50 μM, a statistically significant increase in proliferation was noted. In the presence of **D** and **E**, no cytotoxic activity was observed in the whole concentration range tested. For all compounds at each concentration, the decrease in culture viability was less than 30% compared to the control (i.e., no cytotoxic potential of the tested compounds).

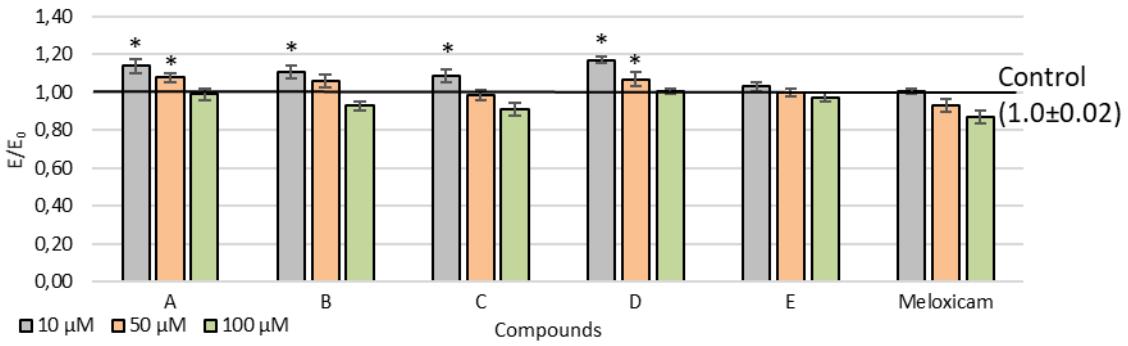

Figure 2. Effect of tested compounds on the viability of NHDF cells; * $p < 0.05$—significant difference compared to control.

2.3. Cyclooxygenase Inhibition

All compounds tested inhibited both COX-1 and COX-2 activity (Table 1). In the case of compounds **A** and **D**, COX-1 inhibition was stronger compared to meloxicam, which was the reference compound. Compounds with COX-2 inhibitory activity (except for **C**) showed higher activity than meloxicam. Most compounds tested (except for **D**) showed stronger COX-2 selectivity than meloxicam. The IC_{50} values obtained for meloxicam are significantly higher than those published by Ogino et al. [19]. However, it was an in vivo study in rats, and we performed only the enzymatic assay. IC_{50} values for tested compounds are similar to those of meloxicam. Therefore in the next stage of research, it is planned to conduct in vivo tests to check the anti-inflammatory properties and gastrointestinal toxicity of the most promising compound **E**.

Table 1. IC_{50} values calculated for COX-1 and COX-2 enzymes after incubation for 2 min with the tested compounds and COX selectivity ratio.

Compound	Cyclooxygenase Inhibition Assay IC_{50} [μM]		COX Selectivity Ratio $IC_{50(COX-2)}/IC_{50(COX-1)}$
	COX-1	COX-2	
A	81.6	54.9	0.67
B	93.2	57.1	0.61
C	95.8	66.2	0.69
D	76.6	56.8	0.74
E	99.2	54.2	0.55
Meloxicam	83.7	59.2	0.71

2.4. Molecular Docking Studies

The empirical scoring function of iGEMDOCK is estimated as E_{total} = Van der Waal's + hydrogen bonding + electrostatic interactions. The docking results are presented in Table 2. The results indicated that compound **D** showed the lowest total binding energy E_{total} with respect to COX-1. The highest value was observed for compound **E**. The docking scores showed a good correlation with IC_{50} values (Table 1). For interactions with COX-2 E_{total} was more negative. The lowest energy was observed for **A** and **E** and the highest for **C**. This result was also in good correlation with inhibitory activity. The compounds with the lowest binding energy showed the most promising biological activity in cyclooxygenase inhibition assay. The molecular docking results also indicated that binding energy of tested compounds were more negative than for meloxicam.

All of the synthesized compounds form 1 to 3 hydrogen bonds with Ser530, Arg120, Leu531, Tyr355 amino acid residues inside COX-1, COX-2 active site, and several hydrophobic interactions (Table 3, Figure 3**).** The COX ligand binding site has four characteristic subdomains **A**–**D** [20]. Subdomain **A** represents the mode of binding of flurbiprofen; subdomain **B** represents the mode of binding of meloxicam and piroxicam; subdomain **C** represents an entrance region of the enzyme binding domain, and subdomain **D** represents the position of the residue in position 523. The most active compound to inhibit COX-1, 4-Methoxy–*N*-[1-(*N*-pyrrolidine)-methyl]-6-methyl-1*H*-pyrrolo[3.4-c]pyridine-1,3(2*H*)-dione (**D**) is bound to enzyme by hydrogen bonds Leu 531 and several hydrophobic interactions, π-sigma with Ala527, π-alkyl with Val349, Leu352, Leu531, Ala527 (Table 3, Figure 3). The main part of the compound, with the pyrrolo-pyridine ring, there is in the subdomain **B** position, the pyrrolidine ring in the entrance region **A**. The position of the molecule is very similar to meloxicam (Figure 4). The most active compound with phenylo-piperazino ring 5,6-dimethyl-4-oxo-2-[(4-phenyl-1-piperazinyl)methyl] -1*H*-pyrrolo[3.4-c]pyridine-1,3(2*H*)-dione is also situated in subdomain **B** (Figure 4**).** It binds by *H*-binding with Ser350 and several hydrophobic interactions (Table 3). The most active compound to inhibit COX-2, 4-Methoxy–*N*-[2-(*N*-morpholine)-ethyl]-6-methyl-1*H*-[pyrrolo[3.4-c]pyridine-1,3(2*H*)-dione is bound to enzyme by hydrogen bonds with Arg120 and Tyr355, and it is stabilized by some several hydrophobic interactions (Figure 3, Table 3). The pyrrolo-pyridine ring takes the position in subdomain **B**, and the morpholine ring is closer region **A** (Figure 4). The most active compound with phenylo-piperazino ring 5,6-dimethyl-4-oxo-2-[(4-phenyl-1-piperazinyl)methyl]-1*H*-pyrrolo[3.4-c]pyridine-1,3(2*H*)-dione, also situated in the subdomain **B** (Figure 4). The orientation in the active site is very similar to the position in COX-1 pocket and meloxicam location.

Table 2. The docking binding energy results for interactions with COX-1 and COX-2.

	COX-1			COX-2		
	Total Binding Energy [kcal/mol]	**Van der Waal's Force [kcal/mol]**	***H* Bond [kcal/mol]**	**Total Binding Energy [kcal/mol]**	**Van der Waal's Force [kcal/mol]**	***H* Bond [kcal/mol]**
A	−105.99	−103.49	−2.50	−118.57	−112.0	−6.57
B	−103.86	−91.78	−12.08	−113.46	−105.35	−8.01
C	−102.84	−88.84	−14.00	−104.42	−100.92	−3.50
D	−107.83	−98.27	−9.56	−112.51	−92.86	−19.65
E	−101.03	−88.20	−12.83	−115.90	−102.53	−13.37
Meloxicam	−102.27	−94.98	−7.29	−104.52	−92.92	−11.60

Table 3. Type of interactions and interacting residues of the COX-1 and COX-2 with compounds **A**–**E**.

	COX-1		COX-2	
	***H*-Bonding**	**Hydrophobic Interactions**	***H*-Bonding**	**Hydrophobic Interactions**
	Residue–Atom of Ligand	**Residue**	**Residue–Atom of Ligand**	**Residue**
A	Ser530-O	Ile345, Val349, Leu352, Leu359, Phe518, Ile523, Gly526, Ala527, Ser530, Leu531	Ser530-O Ser530-O	Ile345, Val349, Leu352, Leu359, Phe518, Met522, Val523, Gly526, Ala527, Ser530, Leu531
B	Ser530-O Arg120-F Arg120-F	Leu93, Val116, Arg120, Val349, Leu352, Tyr355, Tyr385, TRp387, Phe518, Ile523, Gly526, Ala527	Arg120-O	Leu93, Val116, Arg120, Val349, Leu352, Tyr355, Leu359, Val523, Gly526, Ala527
C	Arg120-O	Leu93, Val116, Arg120, Val349, Leu352, Tyr355, Gly526, Ala527	Ser530-O	Ile345, Val349, Leu352, Tyr387, Phe518, Gly526, Ala527, Ser530, Leu531
D	Leu531-O	Arg120, Val349, Leu352, Ile523, Gly526, Ala527, Leu531	Arg120-O Tyr355-N	Arg120, Val349, Tyr355, Ala527, Ser530, Leu531
E	Arg120-O Tyr355-O Tyr355-O	Val116, Val349, Leu352, Tyr355, Tyr385, TRp387, Ile523, Gly526, Ala527	Arg120-O Tyr355-O Tyr355-O	Arg120, Val349, Tyr355, Tyr385, Val523, Gly 526, Ala527

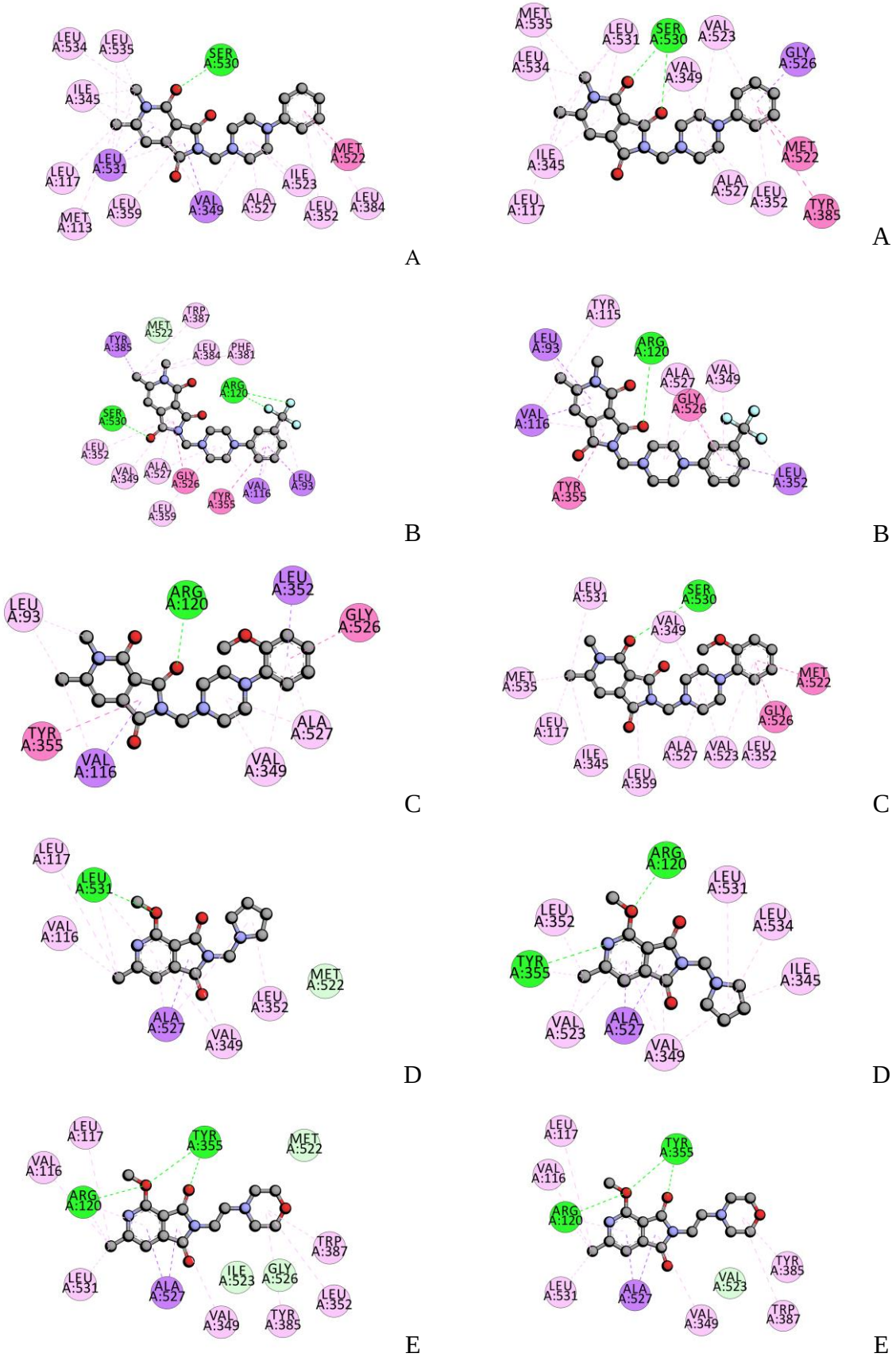

Figure 3. 2D interaction (**A**–**E**) with COX-1 (**left**) and COX-2 (**right**) (green—hydrogen bonds, violet—π-sigma, pink—other hydrophobic).

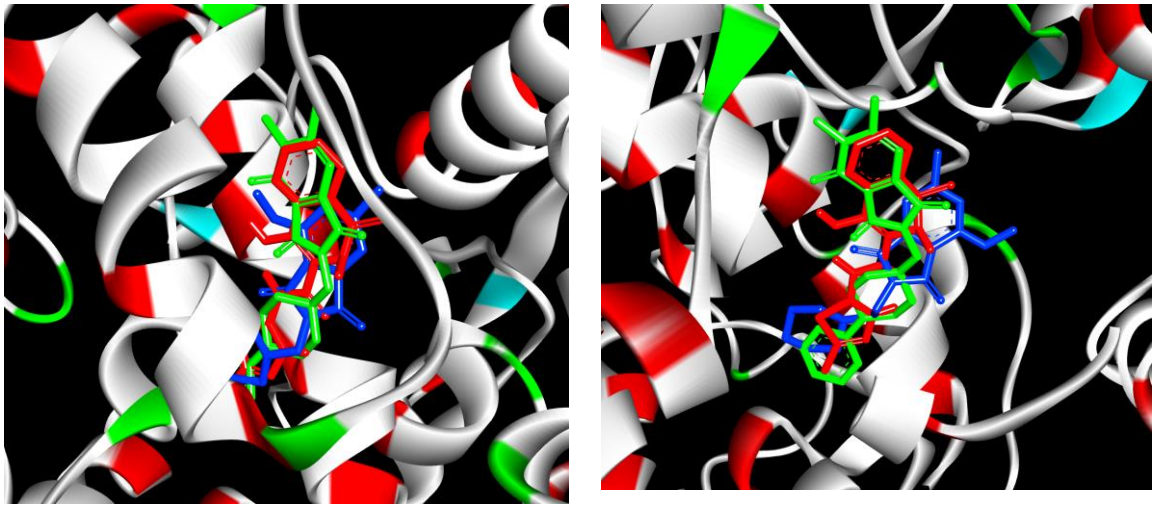

Figure 4. Docking poses of **A** (green), **C** (blue-left), **D** (blue-right) and meloxicam (red) inside COX-1 active site (**left**) and COX-2 active site (**right**).

2.5. Fluorescence Quenching of BSA by Compound **A**–**E**

The steady-state fluorescence spectroscopy and the synchronous fluorescence spectroscopy were used to study fluorescence quenching of BSA by compounds **A**–**E**. The fluorescent behavior of BSA is due to the amino acid residues: Trp, Tyr, and Phe. However, Trp residue has the strongest fluorescence intensity. Thus, the two Trp residues of BSA are mainly responsible for its fluorescence. The fluorescence spectra were recorded for BSA in the presence of studied compounds at the excitation wavelengths λ = 280 nm (both Trp and Tyr residues are excited) and concentration range 0.0–5.0 μM. The fluorescence emission spectra for all tested compounds were shown in Figure 5. The fluorescence intensity of BSA was decreased with increasing concentration of compounds **A**–**E**. The presence of **A**–**E** not only quenched the fluorescence of BSA, but it also caused a blue shift in the maximum emission wavelength of protein. For that, a strong fluorescence emission band at 349 nm, was observed. A careful analysis of the spectra discloses that at a lower concentration of **A**–**E** (**A**–**E**/BSA molar ratio 0.2–2:1), its shift is rather slight, up to 1.5 nm. In the medium range of concentration, change in λ_{max} is more evident. **A** large change in λ_{max} in the presence of a high concentration of **A**–**E** (**A**–**E**/BSA molar ratio 5:1) indicates the unfolding of the polypeptide backbone of macromolecule [21]. The blue shift effect expressed that the conformation of BSA was changed. It also indicated the amino acid residues are located in a more hydrophobic environment and are less exposed to the solvent [22]. Fluorescence quenching and shift of λ_{max} identifies interaction with BSA and can suggest the formation of complexes (static quenching). However, it can also be the result of the collisional encounters (dynamic quenching). In order to confirm the quenching mechanism and complex formation, the fluorescence data were further analyzed by the Stern–Volmer equation and dependence on temperature.

Fluorescence intensities were corrected for the absorption of excitation light and re-absorption of emitted light to decrease the inner filter using the following relationship:

$$F_{corr} = F_{obs} 10^{\frac{(A_{ex}+A_{em})}{2}} \quad (1)$$

where, F_{corr} and F_{obs} are the corrected and observed fluorescence intensities, respectively. A_{ex} and A_{em} are the absorbance values at excitation and emission wavelengths, respectively.

In most cases, the possible quenching mechanism is characterized by a linear Stern–Volmer plot and is usually analyzed using the classical Stern–Volmer Equation (1) [23]:

$$\frac{F_0}{F} = 1 + k_q \tau_0 [Q] = 1 + K_{sv}[Q] \quad (2)$$

where F_0 and F are the steady-state fluorescence intensities at the maximum wavelength in the absence and presence of quencher, respectively, k_q the quenching rate constant of the biomolecule, τ_0 the average lifetime of the biomolecule, [Q] is the quencher concentration, and K_{sv} is the Stern–Volmer constant. For determining the type of quenching liner fitting was analyzed (Figure 6). The average lifetime of the fluorophore in the excited state for a biomolecule is 10^{-8} s [24]. According to Equation (2), the Stern–Volmer constant and the quenching rate constants were obtained from the linear fitting of the experimental data. Received data are collected in Table 4. For dynamic quenching, the maximum scatters collision quenching constant of different quenchers with the biopolymers was reported to 2×10^{10} $dm^3 \cdot mol^{-1} \cdot s^{-1}$ [25]. The results showed that the value of k_q for all cases is much greater, which indicated that the probable quenching mechanism of fluorescence of BSA by **A**–**E** is not caused by a dynamic collision but from the formation of a complex.

The dynamic and static quenching can be distinguished by their dependence on temperature. The higher temperature may result in decreasing stability of the complex and thus smaller values of the static quenching constant. The fluorescence data were analyzed at three different temperatures, and the fluorescence quenching constant of BSA was calculated using the Stern–Volmer Equation (2). The results are listed in Table 4. The Stern–Volmer quenching constant K_{sv} is inversely correlated with temperature, and k_q is much greater than the value of the maximum scatter collision quenching constant. It suggested the formation of ground-state complex and involvement of static quenching between BSA and studied compounds.

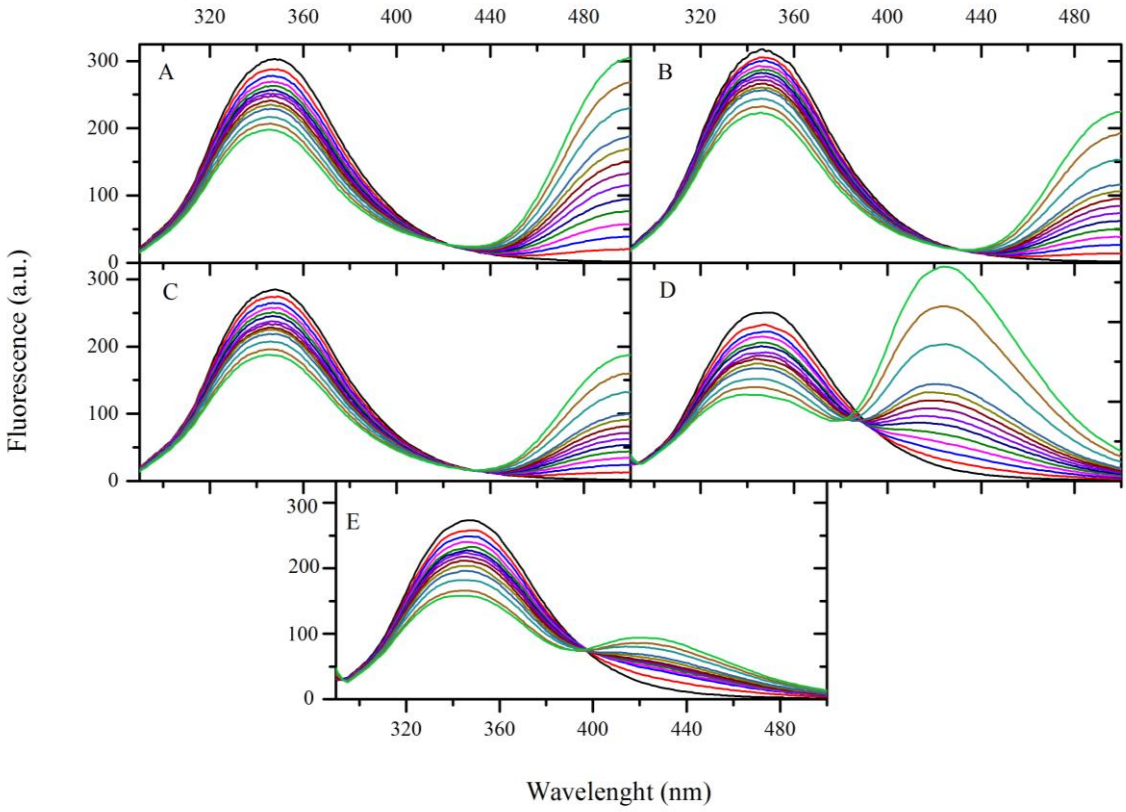

Figure 5. Fluorescence spectra of body surface area (BSA) solution in presence of (**A**–**E**) (T-298 K, λ_{ex} = 280 nm). The concentration of (**A**–**E**) was: 0, 0.2, 0.4, 0.6, 0.8, 1.0, 1.2, 1.4, 1.6, 1.8, 2.0, and 5.0 μM.

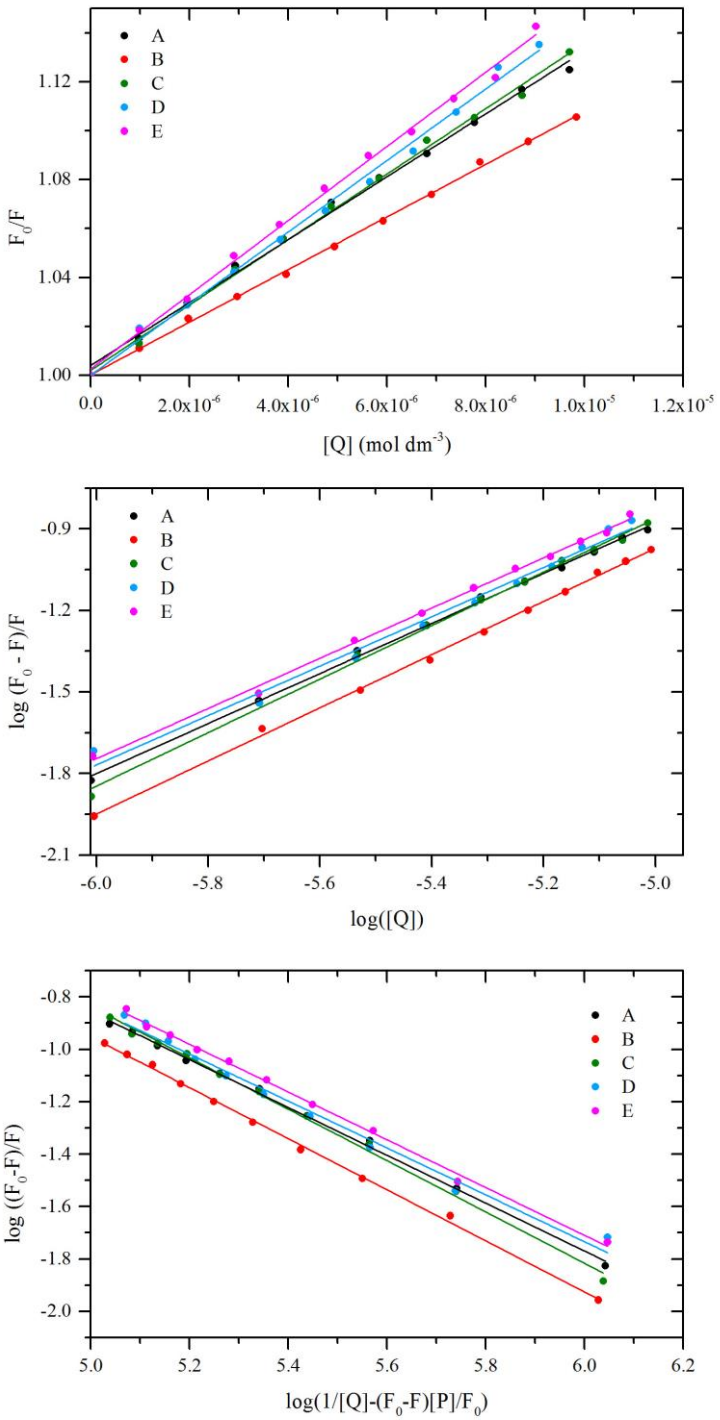

Figure 6. Stern–Volmer plots (**top**), double logarithm regression plots (**middle**), and modified double logarithm regression plots (**bottom**) for quenching of BSA by **A–E**.

Table 4. The Stern–Volmer constant K_{sv} and the quenching rate constant k_q, binding constants K_b and binding stoichiometry n for the interaction of BSA with studied compounds at different temperatures.

		Quenching			Double log			Modified Double log		
	T [K]	$K_{sv} \times 10^4$ [$dm^3 \cdot mol^{-1}$]	$k_q \times 10^{12}$ [$dm^3 \cdot mol^{-1} \cdot s^{-1}$]	R^2	$K_b \times 10^3$ [$dm^3 \cdot mol^{-1}$]	n	R^2	$K_b \times 10^3$ [$dm^3 \cdot mol^{-1}$]	n	R^2
	298	1.28	1.28	0.987	5.37	0.93	0.998	5.23	0.92	0.998
A	303	1.20	1.20	0.997	2.14	0.86	0.997	2.00	0.85	0.993
	310	1.09	1.09	0.992	0.83	0.80	0.993	0.74	0.78	0.996
	298	1.07	1.07	0.996	8.32	0.98	0.998	8.32	0.97	0.998
B	303	1.02	1.02	0.998	3.98	0.92	0.998	3.89	0.91	0.999
	310	0.99	0.99	0.996	1.70	0.85	0.999	1.58	0.84	0.999
	298	1.33	1.33	0.987	11.51	0.98	0.997	11.14	0.98	0.996
C	303	1.30	1.30	0.994	5.25	0.92	0.998	5.01	0.92	0.997
	310	1.28	1.28	0.991	2.24	0.85	0.997	2.04	0.84	0.997
	298	1.46	1.46	0.997	4.82	0.91	0.996	4.34	0.90	0.989
D	303	1.43	1.43	0.996	2.34	0.85	0.997	2.03	0.83	0.997
	310	1.34	1.34	0.991	1.41	0.81	0.999	1.23	0.79	0.998
	298	1.51	1.51	0.998	6.24	0.92	0.997	5.74	0.91	0.997
E	303	1.48	1.48	0.991	3.55	0.87	0.992	3.16	0.86	0.991
	310	1.41	1.41	0.994	1.55	0.82	0.991	1.32	0.80	0.991

2.6. Circular Dichroism Spectra

CD spectroscopy is a very good method to determine the conformational changes in the secondary structure of proteins in case of presence of compounds which can interact with protein molecule [26]. In this study, there were analyzed changes in the secondary structure of BSA in the absence and presence of **A**–**E** compounds. In all CD spectra, two negative bands were observed at near 208 nm and 222 nm, what is characteristic for BSA (Figure 7). It is a typical feature of the α-helical structure of the protein. Any change in this region of spectra suggests conformational changes in protein molecules [27]. Figure 7 shows that in the presence of all analyzed compounds, values of ellipticity at 208 nm and 222 nm decreased after adding every portion of **A**–**E**. These changes suggest a loss in the α-helix(%). Any shift of the peaks was not observed. The content of α-helix can be calculated using Equations (3) and (4) [28]:

$$\alpha - helix(\%) = \frac{-MRE_{208} - 4000}{33000 - 4000} 100\% \quad (3)$$

where MRE_{208} is the observed *MRE* value at 208 nm, 4000, and 33,000 is *MRE* value of the β-form and random coil conformation cross at 208 nm value of pure *α-helix* at 208 nm, respectively.

$$MRE = \frac{ObservedCD(mdeg)}{10Cnl} \quad (4)$$

where *C* is the molar concentration of BSA, *n* is the number of amino acid residues, which is 583 for BSA, *l* is the path length.

All analyzed compounds caused a reduction in the α-helical contents of BSA. The results collected in Table 5 show that the biggest decreasing of α-helix(%) is observed for compound **C**. The α-helical content of BSA decreased here from 61.6% to 44.5% (change 17.1%) with increasing BSA to **C** molar ratio from 1:0 to 1:10 (Table 5, Figure 7). Smaller changes were observed for the interaction of BSA with **A**, **B**, **D**, and **E** compounds. Obtained values for α-helix(%) were changing from 58.7% to 52.8% (change 5.9%) for **A**, 61.8% to 52.8% (change 9%) for **B**, 59.0% to 52.3% (change 7.3%) for **D** and 61.7% to 53.9% (change 7.8%). In all cases, the changes in the molar ratio were the same as in the BSA/**C** system. Therefore, CD studies showed that all analyzed compounds bind to BSA. Obtained results are in agreement with fluorescence spectroscopy.

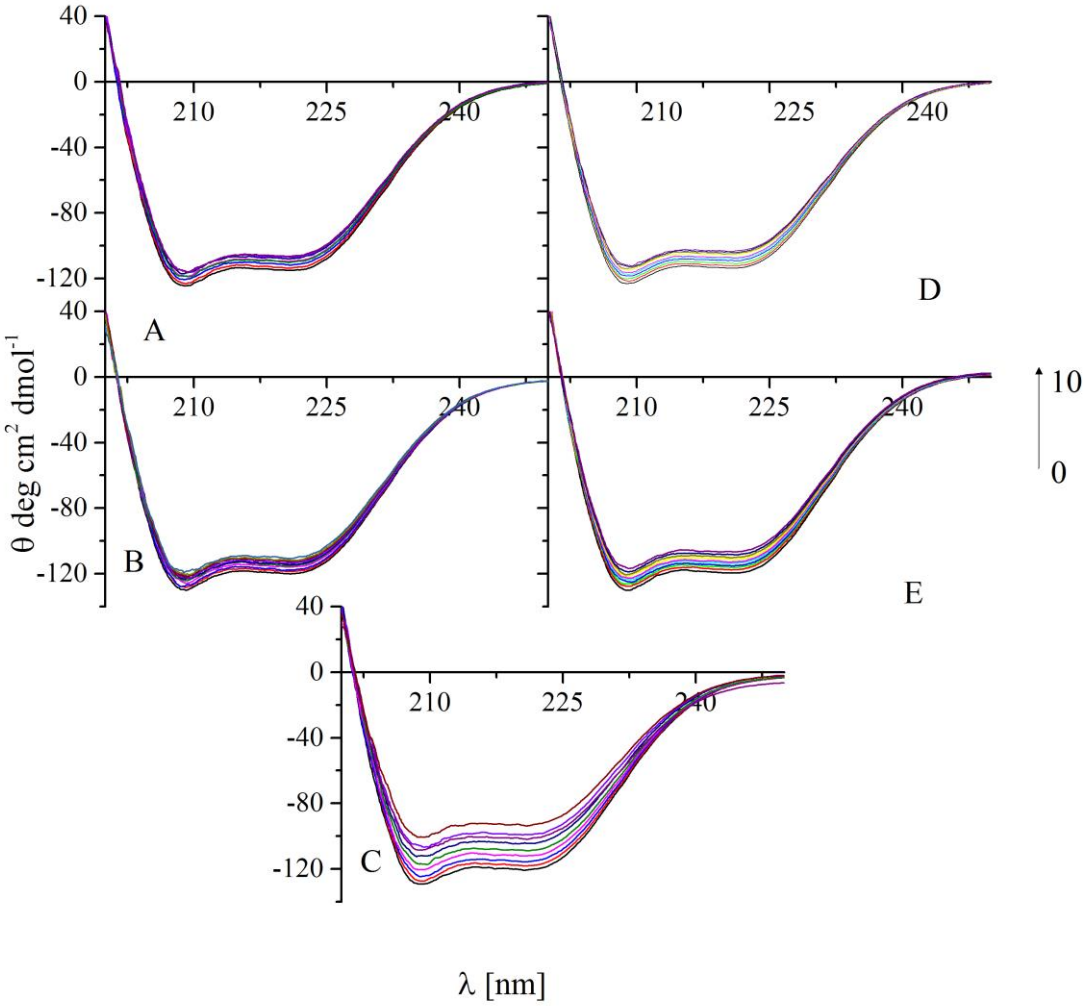

Figure 7. Circular Dichroism (CD) spectra of BSA in the absence and presence of (**A**–**E**) and (**C**). BSA to analyzed compounds molar ratios were changing from 1:0 to 1:10.

Table 5. The values of calculated α-helix(%) for BSA with the absence and presence of **A**–**E**.

	A	**B**	**C**	**D**	**E**
BSA/compound molar ratio			α-helix(%)		
1:0	58.7%	61.8%	61.6%	59.0%	61.7%
1:0.5	57.5%	60.7%	60.1%	57.8%	60.5%
1:1	56.6%	60.6%	58.1%	57.2%	59.9%
1:2	55.0%	58.9%	56.4%	56.0%	58.7%
1:4	54.4%	58.4%	53.9%	54.8%	57.5%
1:6	54.1%	56.7%	48.1%	53.0%	56.3%
1:8	53.1%	53.1%	47.4%	52.6%	55.4%
1:10	52.8%	52.8%	44.5%	52.3%	53.9%

2.7. Binding Constants

For all analyzed systems, the binding constants and the binding stoichiometry were calculated. However, in the literature, there are several models to determine the binding parameters. The values obtained from different methods of calculation could significantly differ from each other [29–31]. Each of them also has various limitations. Two models were used to analyze the received data: double logarithm regression curve (5), modified double logarithm regression curve (6). Using the double

logarithm regression curve, the binding constant $K_{b,}$ and the number of binding stoichiometry n was determined using the following Equation (5) [23]:

$$log\frac{F_0 - F}{F} = logK_b + nlog[Q] \quad (5)$$

where F_0 and F are the steady-state fluorescence intensities at the maximum wavelength in the absence and presence of quencher, respectively, $[Q]$ is the quencher concentration. The corresponding values were obtained from the slope and the intercept of the plot of log $[(F_0 - F)/F]$ versus log $[Q]$. The liner segment, corresponding to **A**–**E** /BSA molar ratio 2:1, was analyzed (Figure 6 and Table 4). The results showed that the binding constant increases in order **A**-**B**-**C**, i.e., when the phenyl ring is substituted (Figure 1). The binding constants for **D** and E are similar and lower than for **B** and **C**. The n value close to 1 shows one to one interaction.

The second method: modified double logarithm regression curve (6), in contrast to the previous one, takes into account the total concentration of protein present in the analyzed solution.

$$log\frac{F_0 - F}{F} = nlogK_b + nlog\frac{1}{[Q] - (F_0 - F)\frac{[P]}{F_0}} \quad (6)$$

where $[P]$ is BSA concentration. By the plot of log $(F_0 - F)/F$ vs. log $(1/([Q] - (F_0 - F)[P]/F_0))$, the binding stoichiometry n and the constant K_b were obtained (Table 4, Figure 6). The results showed that the binding constants and the number of the binding site are slightly smaller than values obtained from Equation (5). It is supposed that the free concentration of the binding compound is not equal to the total concentration of the quencher.

The interaction of 14 anti-inflammatory drugs with human serum albumin was investigated by F. Mohammadnia [32]. The binding constants were found with the range 10^2 $dm^3 \cdot mol^{-1}$ (acetaminophen) to 1.88×10^7 $dm^3 \cdot mol^{-1}$ for meloxicam. So, K_b values of studied compounds show that the interactions with BSA is moderate. Similar values were obtained for many compounds with biological activity. For example, series of flavonoids (binding constants in the range $1–15 \times 10^4$) [33], a lipophilic derivative of thalidomide (anti-inflammatory agent) [34], a pyrimidine derivative (antibacterial reagent) [35], an indole derivative (COX inhibitor) [36] or a bis-isatin derivative (potential anti-proliferative activity) [37].

2.8. Thermodynamic studies

The interaction forces between a small molecule and protein include hydrogen bond, van der Waals force, electrostatic and hydrophobic interactions, etc. [38]. The forces involved in the interaction are identified by the thermodynamic analysis. The signs and magnitudes of the thermodynamic parameters identify the type of interactions [39]. The enthalpy change (ΔH°), the entropic change (ΔS°) and free energy change (ΔG°) were calculated from Equations (7) and (8):

$$logK_b = -\frac{\Delta H^\circ}{RT} + \frac{\Delta S^\circ}{R} \quad (7)$$

$$\Delta G^\circ = \Delta H^\circ - T\Delta S^\circ = -RTlnK_b \quad (8)$$

where K_b is the binding constant, R is the universal gas constant.

The calculated data for all compounds are presented in Table 6. The results showed that the binding interaction between tested compounds and BSA were spontaneous due to the negative ΔG° values at the studied temperature range. Furthermore, both the ΔH° and ΔS° negative values indicate that the main interaction force in the binding process was van der Waals forces and/or hydrogen bonding interaction.

Table 6. Binding and thermodynamic parameters for the binding interaction between **A–E** and BSA.

	T [K]	logK_b	n	R^2	ΔG° [kJmol^{-1}]	ΔH° [kJmol^{-1}]	ΔS° [Jmol^{-1}K^{-1}]
	298	3.73 ± 0.07	0.93 ± 0.01	0.998			
A	303	3.33 ± 0.13	0.86 ± 0.04	0.997	−21.16	−11.88	−327.53
	310	2.87 ± 0.16	0.80 ± 0.03	0.993			
	298	3.92 ± 0.07	0.98 ± 0.01	0.998			
B	303	3.60 ± 0.06	0.92 ± 0.01	0.998	−22.28	−10.00	−260.88
	310	3.23 ± 0.03	0.85 ± 0.01	0.999			
	298	4.06 ± 0.09	0.98 ± 0.02	0.997			
C	303	3.72 ± 0.08	0.92 ± 0.02	0.998	−23.07	−10.38	270.95
	310	3.35 ± 0.08	0.85 ± 0.02	0.997			
	298	3.68 ± 0.10	0.91 ± 0.03	0.996			
D	303	3.37 ± 0.07	0.85 ± 0.01	0.997	−20.83	−7.73	−189.67
	310	3.15 ± 0.05	0.81 ± 0.01	0.999			
	298	3.80 ± 0.08	0.92 ± 0.02	0.997			
E	303	3.55 ± 0.12	0.87 ± 0.03	0.992	−21.68	−8.92	−226.56
	310	3.19 ± 0.15	0.82 ± 0.03	0.991			

2.9. Site Markers Studies

BSA, as well as human serum albumin (HSA), is known to possess two binding sites (a site I, site II), which are situated in subdomains IIA and IIIA, respectively [40]. To evaluate the binding site in BSA for **A–E**, displacement studies were carried out by using phenylbutazone (PHB) and ibuprofen (IBP) as site probes. The site I shows the binding affinity towards PHB, site II is known to bind IBP [41]. Fluorescence emission spectra of the mixed solutions of BSA and site markers following a concentration increment of **A–E** were recorded. Quenching rate and binding constants were analyzed using Equation (2) and (5). The results were summarized in Table 7. Results show that both K_b and k_q values of compounds **A–C** with BSA in the presence of IBP, considerably decrease compared to without IBP. In the case of PHB, changes were slight. It can be concluded that **A–C** binds to subdomain IIIA of BSA. For **D** and **E**, that binding constant in the presence of PHB and IBU considerably decline compared to without markers. It can be concluded that **D** and **E** may bind to subdomain IIA or IIIA of BSA. However, it seems that the IBP site is more preferred, especially for molecule **E**.

Table 7. The binding constant of **A–E** with co-solution of BSA and site markers.

System	K_b [dm^{3}mol^{-1}]	R^2	K_q [dm^{3}mol^{-1}]	R^2
BSA+A	5.37×10^3	0.998	1.28×10^{12}	0.996
BSA+A+PHB	5.12×10^3	0.983	1.22×10^{12}	0.982
BSA+A+IBP	1.17×10^3	0.982	5.46×10^{11}	0.977
BSA+B	8.32×10^3	0.998	1.07×10^{12}	0.995
BSA+B+PHB	8.16×10^3	0.981	1.01×10^{12}	0.982
BSA+B+IBP	1.02×10^3	0.986	3.81×10^{11}	0.991
BSA+C	1.15×10^4	0.997	1.33×10^{12}	0.987
BSA+C+PHB	1.02×10^4	0.985	1.28×10^{12}	0.989
BSA+C+IBP	5.82×10^3	0.975	6.97×10^{11}	0.976
BSA+D	4.82×10^3	0.996	1.46×10^{12}	0.997
BSA+D+PHB	1.50×10^2	0.987	5.11×10^{11}	0.988
BSA+D+IBP	1.38×10^2	0.981	1.51×10^{11}	0.983
BSA+E	6.24×10^3	0.997	1.51×10^{12}	0.998
BSA+E+PHB	4.74×10^2	0.985	1.22×10^{11}	0.985
BSA+E+IBP	1.94×10^2	0.969	1.03×10^{11}	0992

2.10. Molecular Docking-Interactions with BSA

In order to determine the preferred binding sites of the compounds **A**–**E** on BSA, the binding interactions were simulated by the molecular docking method. The simulated results were presented in Table 8. As is well known, the more negative the binding free energy ΔG°, the more stable the formed complex is. The results revealed that the binding free energy for **A**–**C** within the hydrophobic cavity in site II (subdomain IIIA) of BSA was more negative than that within the hydrophobic cavity in the site I (subdomain IIA). This indicating that site II is favorable. For **D** and **E**, the binding free energy ΔG° within site I and site II are close to each other. It indicates that both site are favorable. This result is consistent with the results observed in the site marker fluorescence studies. As presented in Table 8, the sum of van der Waals energy, hydrogen bonding energy, and desolvation free energy (ΔE_2) is more negative than electrostatic energy (ΔE_3). Hence, it can indicate that the main interactions between compounds **A**–**C** and BSA are van der Waals and hydrogen bonding interactions. Our thermodynamic studies also indicated that van der Waals and hydrogen bonding contributed to the interaction of the BSA-tested compound. In binding sites, II studied compounds insert into the hydrophobic cavity are surrounded by various kinds of residues (Figure 8). Hydrogen bonds with Arg208, Leu480 are formed. In the site, I pocket also hydrogen bonds are formed (Arg-217, Gly-220, Val-342). The π-sigma and other hydrophobic interactions are observed. Tryptophan residue (Trp-213) is close to tested compounds. The details are presented in Figure 8.

Table 8. Energies of the binding complexes obtained from molecular docking.

	Binding Site	ΔG° [kJmol^{-1}]	ΔE_1 [kJmol^{-1}]	ΔE_2 [kJmol^{-1}]	ΔE_3 [kJmol^{-1}]
A	site I	−31.50	−32.23	−31.50	−3.77
	site II	−35.56	−39.28	−35.06	−4.22
B	site I	−29.29	−34.26	−30.63	−3.64
	site II	−35.14	−40.12	−35.68	−4.39
C	site I	−31.42	−36.40	−33.26	−3.13
	site II	−36.52	−41.54	−37.57	−3.93
D	site I	−26.70	−30.41	−26.98	−3.55
	site II	−27.44	−31.21	−26.94	−4.23
E	site I	−26.52	−31.51	−27.57	−4.14
	site II	−27.48	−32.46	−28.53	−3.93

ΔG°—binding free energy; ΔE_1—intermolecular interaction energy, which is the sum of van der Waals energy, hydrogen bonding energy, desolvation free energy and electrostatic energy; ΔE_2—the sum of Van der Waals energy, hydrogen bonding energy and desolvation free energy; ΔE_3—electrostatic energy.

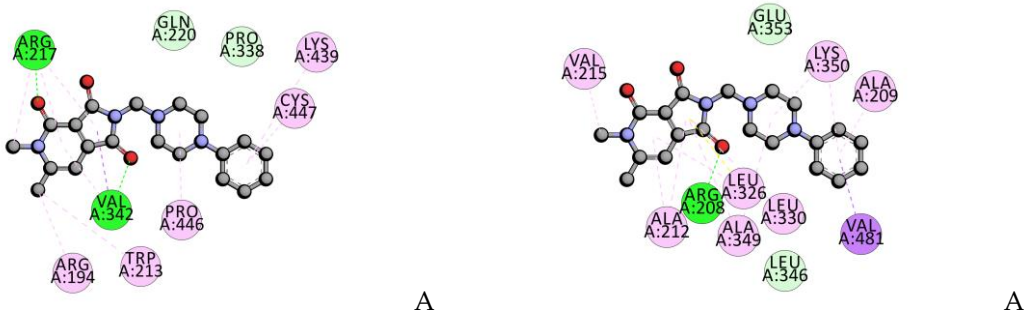

Figure 8. *Cont.*

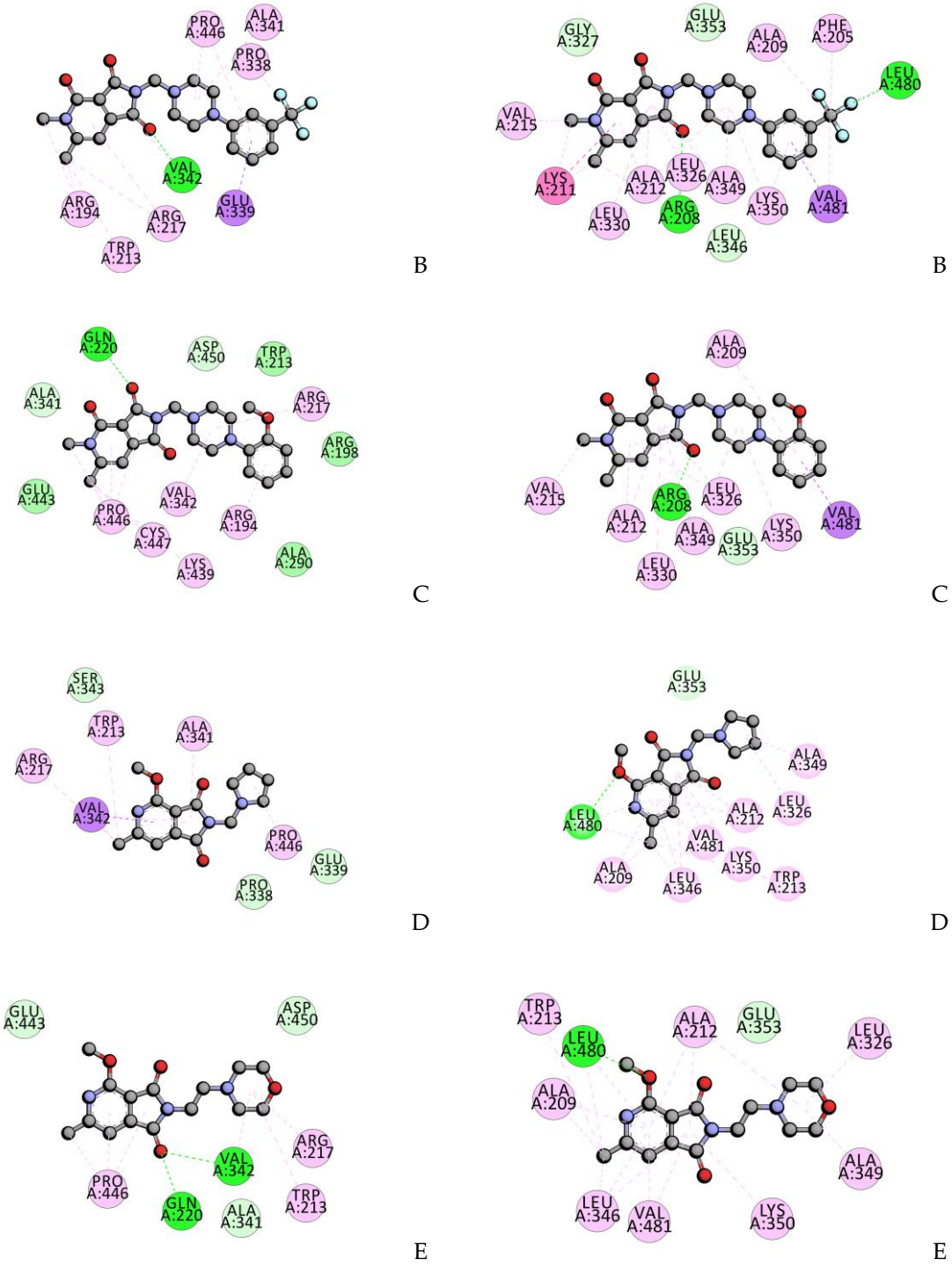

Figure 8. 2D interaction of (**A**–**E**) with BSA in the binding site I (**left**) and site II (**right**) (green—hydrogen bonds, violet—π-sigma, pink—other hydrophobic).

3. Materials and Methods

3.1. Chemistry

All the results of **C**, **H**, **N** determinations were within ±0.4% of theoretical values, carried out by Carlo Erba Elemental Analyzer model NA-1500 (Carlo Erba, Thermo Scientific, Waltham, MA, USA). ^{1}H NMR spectra were determined in DMSO (**A**–**C**) or $CDCl_3$ (**D** and **E**) on a Bruker 300 MHz NMR spectrometer (Bruker, Billerica, MA, USA), using TMS as an internal standard. FTIR spectra were

run on Perkin-Elmer Spectrum Two, UATR FT-IR spectrometer (Perkin Elmer, Waltham, MA, USA). The samples were applied as solid.

3.1.1. General Method for the Preparation of the Mannich Bases **A**–**C** (Scheme 1)

A 0.6 g (0.0031 mol) 1,6-dimethyl-3,4-pyridinedicarboximide 2 was dissolved in 40 mL of tetrahydrofurane and to this suspension 1 mL 33% formaline was added. This mixture was refluxed for 0.5 h. After this time 0.0035 mol of suitable *N*-arylpiperazines were added, again refluxed for 10 h. After one hour this mixture was cleared and other 2 more hours the products started to precipitate. The reactions were monitored by TLC. The separated solid substance was collected on a filter and washed with diethyl ether and dried (crude). The analytical samples were obtained after crystallization from distilled water (**A**) or THF (**B** and **C**). The properties of obtained compounds **A**–**C** show below (^{1}H NMR plots are available in supplementary file):

A: 5,6-dimethyl-4-oxo-2-[(4-phenyl-1-piperazinyl)methyl]-1*H*-pyrrolo[3.4-c]pyridine-1,3(2*H*)-dione: $C_{20}H_{22}N_4O_3$, m.w. 366.46, m.p. 250 °C, solvent distilled water, THF, yield 93.86%; TLC R_f = 0.1 (ethyl acetate); R_f = 0.81 (ethyl acetate: methanol 1:1) ^{1}H NMR δ: 2.37 (s-3*H*, CH_3 at **C**-6), 2.55–2.65 (m-4*H*, -CH_2-*N*-(CH_2)$_2$-); 3.05–3.15 (m-4*H*, -(CH_2)$_2$-*N*-C_6H_5); 3.30 (s-3*H*, *N*-CH_3); 4.39 (s-2*H*, -*N*-CH_2-*N*-); 6.53 (s-1*H*, *H* arom. of pyridine); 6.70–6.75 (t-1*H*, arom *p*-*H* of benzene); 6.85–6.88 (d-2*H*, *o*-*H* of benzene); 7.13–7.18 (t-2*H*, *m*-*H* of benzene). FT-IR: *C*=*O* 1660; 1714; 1750 [cm^{-1}], monosubstituted benzene 770, 700.

B: 5,6-dimethyl-4-oxo-2-[4-(3-trifluormethyl)phenyl-1-piperazinyl)methyl]-1*H*-pyrrolo[3.4-c]pyridine -1,3(2*H*)-dione: $C_{21}H_{21}N_4O_3F_3$, m.w. 434.46, m.p. 267 °C, solvent THF; yield 86.29%; TLC R_f = 0.08 (ethyl acetate); R = 0.79 (ethyl acetate: methanol 1:1); ^{1}H NMR δ: 2.37 (s-3*H*, CH_3 at **C**-6), 2.55–2.65 (m-4*H*, -CH_2-*N*-(CH_2)$_2$-); 3.15–3.25 (m-4H, -(CH_2)$_2$-*N*-C_6H_4-CF_3); 3.30 (s-3*H*, *N*-CH_3); 4.40 (s-2*H*, -*N*-CH_2-*N*-); 6.54 (s-1*H*, *H* arom of pyridine.), 7.10–7.37 (m-3*H*, *H* arom. of benzene). FT-IR: *C*=*O* 1660; 1714; 1757 [cm^{-1}]; m-disubstituted benzene 700, 784.

C: 5,6-dimethyl-4-oxo-2-[4-(2-methoxy)phenyl-1-piperazinyl)methyl]-1*H*-pyrrolo[3.4-c]pyridine-1,3(2*H*)-dione: $C_{21}H_{24}N_4O_4$, m.w. 396.49, m.p. 234 °C, crude(insoluble on etanol, methanol; diethyl ether, $CDCl_3$); yield 79.41%; TLC R_f = 0.06 (ethyl acetate); R_f = 0.75 (ethyl acetate: methanol 1:1); ^{1}H NMR δ: 2.38 (s-3*H*, CH_3 at **C**-6), 2.55–2.65 (m-4*H*, -CH_2-*N*-(CH_2)$_2$-); 2.85–2.95 (m-4*H*, -(CH_2)$_2$-*N*-C_6H_4-OCH_3); 3.30 (s-3*H*, *N*-CH_3); 3.71 (s-3*H*, -*O*-CH_3), 4.40 (s-2*H*, -*N*-CH_2-*N*-); 6.55 (s-1*H*, *H* arom. of pyridine), 6.82–6.91 (m-3*H*, arom. of benzene). FT-IR: *C*=*O* 1660; 1710; 1750 [cm^{-1}], disubstituted benzene 740.

3.1.2. Method for the Preparation of the imides **D**, **E** (Scheme 1)

A 0.002 mol of 4-methoxy-6-methyl-1*H*-pyrrolo[3.4-c]pyridine-1,3(2*H*)-dion was dissolved in 40 mL of tetrahydrofurane and to this solution 0.4 mL of 33% formaline was added. This mixture was refluxed for 0.5 h. After this time 0.0022 mol of pyrrolidine was added, again refluxed for 10 h. Then, solvent was evaporated completely under reduced pressure. The residue was purified by crystallization from n-Hepxane.

D: 4-Methoxy–*N*-[1-(*N*-pyrrolidine)-methyl]-6-methyl-1*H*-pyrrolo[3.4-c]pyridine-1,3(2*H*)-dione $C_{14}H_{17}N_3O_3$, m.w. 275.35, m.p. 123 °C, solvent n-Hexane; Yeld 60%; ^{1}H NMR δ: 1.691–0.76 (t-4*H*, 2CH_2 pyrrolidine), 2.602–0.79 (m-7*H*, (CH_2)$_2$-*N* and CH_3), 4,13 (s-3*H*, OCH_3), 4.70 (s-2*H*, CH_2), 7.19 (s-1*H*, *H* arom. of pyridine). FT-IR: *C*=*O* 1720, 1770 [cm^{-1}]. (^{1}H NMR plots are available in supplementary file):

A 0.02 mol of potassium was dissolved in 100 mL of anhydrous ethanol and to this solution 0.01 mol of 4-methoxy-6-methyl-1*H*-pyrrolo[3,4-c]pyridine-1,3(2*H*)-dione was added. The reaction mixture was refluxed for 15 min to the obtained suspension, next 0.012 mol of 4-(2-Chloroethyl)morpholine hydrochloride was added. The mixture was refluxed until the alkaline reaction disappeared. After filtration ethanol was evaporated to a small volume and was left to crystallize. The separated product was collected on a filter and purified by crystallization from ethanol.

E: 4-Methoxy–*N*-[2-(*N*-morpholine)-ethyl]-6-methyl-1*H*-[pyrrolo[3.4-c]pyridine-1,3(2*H*)-dione $C_{15}H_{19}N_3O_4$, m.w. 305.37, m.p. 151 °C, solvent ethanol, Yeld 50%; ^{1}H NMR δ: 2.40–2.63 (m-9*H*,

(CH_2)$_3$-*N* and CH_3), 3.60–3.63 (m-4*H*, (CH_2)$_2$-*O* of morpholine), 3.75–3.79 (m-2*H*, CH_2 α), 4.13 (s-3*H*, OCH_3), 7.18 (s-1*H*, *H* arom. of pyridine). FT-IR: *C=O* 1710, 1760 [cm^{-1}] (^{1}H NMR plots are available in supplementary file).

3.2. Cell Line

The study was carried out using the NHDF cell line obtained from ATCC (Manasas, VA, USA). Cells were cultured at 37 °C in a humidified 5% CO_2/95% air atmosphere incubator and passaged twice a week.

The cells were cultivated in DMEM without phenol red supplemented with 10% fetal bovine serum (FBS), 2 mM L-glutamine, 1.25 μg/mL amphotericin B and 100 μg/mL gentamicin. Prepared culture medium was stored at 4–8 °C for up to one month.

3.3. Tested Compounds

Tested were dissolved in DMSO to a stock concentration of 10 mM. All prepared stock solutions were stored at −20 °C for up to 6 months. For the experiment, the above-mentioned tested compounds were used in the concentration range of 10, 50, and 100 μM. Before using, all compounds were dissolved in the medium, and the final DMSO concentration did not exceed 1%.

3.4. MTT Assay

The MTT assay was used to measure the effect of tested compounds on the viability of NHDF cells. After incubation with the compound, the supernatant was removed, 1 mg/mL MTT solution in MEM was added, and plates were incubated for 2 h at 37 °C. The medium was then removed. Formazan crystals were dissolved in 100 μL of isopropanol for 30 min, and absorbance was measured at 570 nm using Varioskan LUX microplate reader (Thermo Scientific).

3.5. Cyclooxygenase Inhibition Assay

COX peroxidase activity was estimated using the ready-to-use kit (Cayman, cat. no. 701050 in triplicate for all compounds at a concentration of 100 μM. Evaluation of the peroxidase activity after 2 min incubation at RT was performed using Varioskan LUX microplate reader (Thermo Scientific, Waltham, MA, USA) at 590 nm. The results are presented as the IC_{50} values, i.e., the concentrations at which 50% inhibition of enzyme activity occurred, separately for COX-1 and COX-2. The selectivity of inhibition of cyclooxygenases was presented as ratios of IC_{50} values (COX-2/COX-1). Meloxicam was used as a reference compound with COX-2 selectivity.

3.6. Statistical Analysis

All results are presented as mean ± SEM (standard error of the mean) expressed as E/E_0 ratio, where E is the culture with the addition of the tested substance, and E_0 is the control without compound. Statistical significance was calculated compared to the control.

Due to the lack of normal distribution, the non-parametric Kruskal-Wallis test was used (with appropriate post-hoc tests). In all assays, $p < 0.05$ was used as the significance level

3.7. Spectroscopic Studies

All the fluorescence measurements were carried out on a Cary Eclipse 500 spectrophotometer (Agilent, Santa Clara, CA, USA,). The interaction between synthesized compounds and bovine serum albumin (BSA) was studied in pH = 7.4 and a concentration of BSA 5.0×10^{-6} mol·dm^{-3}. A solution of BSA was titrated by successive additions 1.0×10^{-3} mol·dm^{-3} solution of studied compounds, to give a final concentration 0.2×10^{-6}–5.0×10^{-6} mol·dm^{-3}. All experiments were measured at three temperatures: 298, 303, and 310 K. Fluorescence quenching spectra were obtained at excitation and an emission wavelength of 280 nm and 300–500 nm, respectively. The following molar ratio **A**–**E**/BSA were:

0.2–2.0 with 0.2 step, 2.0–5.0 with 1.0. Binding displacement studies were carried out in the presence of the two site markers, phenylbutazone (PHB) and ibuprofen (IBP), as sites I and II markers, respectively. Concentrations of BSA and site markers were set at 5.0×10^{-6} and 10.0×10^{-6} mol dm^{-3}, respectively.

Circular dichroism spectra of all BSA solutions under simulated physiological conditions in pH 7.4 in the absence and presence of analyzed compounds were made in room temperature on Jasco J-1500 magnetic circular dichroism spectrometer (Jasco, Tokyo, Japan). 10 mm pathlength was used. CD spectra were collected at a scan rate speed of 50 nm min^{-1} with a response time of 1 s. Measurements were made in the range of 200–250 nm. All spectra were baseline corrected, and the final plot was taken from three accumulated plots. The concentrations of BSA and **A**–**E** compounds were 1.0×10^{-6} mol dm^{-3} and 1.0×10^{-3} mol·dm^{-3}, respectively. Experiments were performed for BSA to each analyzed compound in molar ratios from 1:0 to 1:10.

3.8. Molecular Docking

The ground state geometric optimizations were calculated using density functional theory (DFT) with Becke's three-parameter hybrid exchange function with the Lee-Yang–Parr gradient corrected correlation (B3LYP) [42–44] functional in combination with 6–311+G (d,p) basis set. Calculations were carried out using the Gaussian 2016 A.03 software package [45].

The high-resolution crystal structure of COX-1 and COX-2 co-crystallized with meloxicam and crystal structure of BSA were selected for docking studies (Protein Data Bank, PDB ID: 4O1Z, 4M11 [46]). The interactions with COX-1, COX-2 were performed using iGEMDOCK v.2.1 software [47]. Genetic algorithm (GA) parameters were set as 800 population size, 80 generations in 10 number of solutions. After the molecular docking, the ligand-receptor complexes were further analyzed using Discovery Studio software (http://accelrys.com/). The crystal structure of BSA with PDB ID 3V03 was obtained from Protein Data Bank (http://www.rcsb.org). All the ligands and water molecules were removed, and then hydrogen atoms were added to the protein structure. The intermolecular interactions with BSA were simulated by the molecular docking method implemented in AutoDock 4.2.6 software (http://autodock.scripps.edu/resources/references). The grid maps of dimensions $60 \times 60 \times 60$ with a grid point spacing of 0.375 Å were calculated using AutoGrid. The centers of grid boxes were set according to the binding sites phenylbutazone (PDB ID: 2BXC) and ibuprofen (PDB ID: 2BXG) on HSA ([48]). The running times of the genetic algorithm and the evaluation times were set to 100 and 2.5million, respectively.

4. Conclusions

In this paper, new derivatives of pyridine-1,3(2*H*)-diones were synthesized and evaluated for their COX-I/II activity and interaction with BSA. The result of the COX-1 and COX-2 inhibitory studies revealed that all the compounds potentially inhibited COX-1 and COX-2. The selectivity index was found to be similar to meloxicam. Structural modifications did not significantly affect tested compounds activity. The docking studies were found to be in good correlation with the experimental data, and the pyrrolo-pyridine ring plays an important role in interacting with the enzyme. The experimental results showed that the fluorescence quenching of BSA by studied compounds was a result of complex formation. The values of binding constants also confirm the binding of analyzed derivatives to BSA. These results provide a valuable starting point for the design and synthesis of pyrrolo-pyridine analogs that inhibit COX as potential drugs.

Supplementary Materials: NMR spectra are available online.

Author Contributions: E.K. conceptualization, supervision, performed fluorescence experiments and data analysis, performed molecular docking studies; D.S. performed the synthetic experiments; B.W. performed the biological tests and data analysis; T.G. funding acquisition; A.M. performed CD experiments and data analysis. All authors wrote the manuscript. All authors have read and agreed to the published version of the manuscript.

Funding: The publication was prepared under a project financed from funds granted by the Ministry of Science and Higher Education in the "Regional Initiative of Excellence" program for the years 2019–2022, project number 016/RID/2018/19, the amount of funding PLN 11 998 121.30.

Acknowledgments: Calculations have been carried out in Wroclaw Centre for Networking and Supercomputing (http://www.wcss.wroc.pl).

Conflicts of Interest: The authors declare no conflict of interest.

Abbreviations

COX	Cyclooxygenases
BSA	bovine serum albumin
HSA	human serum albumin
TLC	thin layer-chromatography
THF	Tetrahydrofuran
CD	circular dichroism
DMSO	dimethyl sulfoxide
NHDF	Normal Human Dermal Fibroblasts

References

1. Bailleux, V.; Vallée, L.; Nuyts, J.; Vamecq, J. Synthesis and anticonvulsant activity of two N-(2, 6-dimethylphenyl) pyridinedicarboximides. *Biomed. Pharmacother.* **1995**, *49*, 75–78. [CrossRef]
2. Da Settimo, A.; Primofiore, G.; Da Settimo, F.; Simorini, F.; La Motta, C.; Martinelli, A.; Boldrini, E. Synthesis of pyrrolo[3,4-c]pyridine derivatives possessing an acid group and their in vitro and in vivo evaluation as aldose reductase inhibitors. *Eur. J. Med. Chem.* **1996**, *31*, 49–58. [CrossRef]
3. Deraeve, C.; Dorobantu, I.M.; Rebbah, F.; Le Quéméner, F.; Constant, P.; Quémard, A.; Bernardes-Génisson, V.; Bernadou, J.; Pratviel, G. Chemical synthesis, biological evaluation and structure–activity relationship analysis of azaisoindolinones, a novel class of direct enoyl-ACP reductase inhibitors as potential antimycobacterial agents. *Bioorg. Med. Chem.* **2011**, *19*, 6225–6232. [CrossRef] [PubMed]
4. Zhao, X.Z.; Maddali, K.; Metifiot, M.; Smith, S.J.; Vu, B.C.; Marchand, C.; Hughes, S.H.; Pommier, Y.; Burke, T.R. Bicyclic Hydroxy-1H-pyrrolopyridine-trione Containing HIV-1 Integrase Inhibitors. *Chem. Biol. Drug Des.* **2012**, *79*, 157–165. [CrossRef]
5. Vane, J.R.; Botting, R.M. Anti-inflammatory drugs and their mechanism of action. *Inflamm. Res.* **1998**, *47*, 78–87. [CrossRef]
6. Martel-Pelletier, J.; Lajeunesse, D.; Reboul, P.; Pelletier, J.P. Therapeutic role of dual inhibitors of 5-LOX and COX, selective and non-selective non-steroidal anti-inflammatory drugs. *Ann. Rheum. Dis.* **2003**, *62*, 501–509. [CrossRef]
7. Zarghi, A.; Arfaei, S. Selective COX-2 inhibitors: A review of their structure-activity relationships. *Iran. J. Pharm. Res.* **2011**, *10*, 655–683.
8. Turini, M.E.; DuBois, R.N. Cyclooxygenase-2: A therapeutic target. *Annu. Rev. Med.* **2002**, *53*, 35–57. [CrossRef]
9. Śladowska, H.; Filipek, B.; Szkatuła, D.; Sabiniarz, A.; Kardasz, M.; Potoczek, J.; Sieklucka-Dziuba, M.; Rajtar, G.; Kleinrok, Z.; Lis, T. Investigations on the synthesis and pharmacological properties of 4-alkoxy-2-[2-hydroxy-3-(4-aryl-1-piperazinyl)propyl]-6-methyl-1H-pyrrolo[3,4-c]pyridine-1,3(2H)-diones. *Farmaco* **2003**, *57*, 897–908. [CrossRef]
10. Sladowska, H. Investigations on the synthesis and properties of arylpiperazinylalkyl derivatives of some dihydro- and tetrahydropyrido[2,3-d]pyrimidines. *Farmaco* **1993**, *48*, 77–84. [CrossRef]
11. Johnson, R.S.; Lovett, T.O.; Stevens, T.S. The alkaloids of Gelsemium sempervirens. Part IV. Derivatives of pyridine, isoquinoline, and indol-2(3H)-one as possible initial materials for synthesis of gelsemine. *J. Chem. Soc. C Org.* **1970**, *6*, 796. [CrossRef]
12. Von Dobeneck, H.; Hansen, B. Aza-isoindole, I Aza-phthalimidine. *Chem. Ber.* **1972**, *105*, 3611–3621. [CrossRef]

13. Sladowska, H.; Szkatuła, D.; Filipek, B.; Maciag, D.; Sapa, J.; Zygmunt, M. Synthesis and properties of 2-(4-substituted)butyl derivatives of some 2,3-dihydro-1,3-dioxo-1H-pyrrolo[3,4-c]pyridines. *Pharmazie* **2001**, *56*, 133–138. [CrossRef] [PubMed]
14. Śladowska, H.; Potoczek, J.; Sokołowska, M.; Rajtar, G.; Sieklucka-Dziuba, M.; Kocki, T.; Kleinrok, Z. Investigations on the synthesis and properties of N-phenyl derivatives of 1,4-dioxo (1,4,5-trioxo)-1,2,3,4-tetra (1,2,3,4,5,6-hexa) hydropyrido- [3,4-d] pyridazines and allied compounds. *Farmaco* **1998**, *53*, 468–474. [CrossRef]
15. Śladowska, H.; Stanasiuk, J.; Sieklucka-Dziuba, M.; Saran, T.; Kleinrok, Z. Investigations on the synthesis and properties of 4-aminosubstituted 2,6,7-trimethyl-1,5-dioxo-1,2,5,6-tetrahydropyrido [3,4-d] pyridazines. *Farmaco* **1998**, *53*, 475–479. [CrossRef]
16. Roman, G. Mannich bases in medicinal chemistry and drug design. *Eur. J. Med. Chem.* **2015**, *89*, 743–816. [CrossRef]
17. Śladowska, H.; Filipek, B.; Szkatuła, D.; Sapa, J.; Bednarski, M.; Ciołkowska, M. Investigations on the synthesis and pharmacological properties of N-substituted derivatives of 4-alkoxy-6-methyl-1H-pyrrolo [3,4-c]pyridine-1,3(2H) -diones. *Farmaco* **2005**, *60*, 53–59. [CrossRef]
18. Sladowska, H.; Sabiniarz, A.; Szkatula, D.; Filipek, B.; Sapa, J. Synthesis and properties of 4-alkoxy-2-[2-hydroxy-3-(4-o,m,p-halogenoaryl-1 -piperazinyl)propyl]-6-methyl-1H-pyrrolo-[3,4-c]pyridine-1,3(2H)-diones with analgesic and sedative activities. *Acta Pol. Pharm.* **2006**, *63*, 245–254.
19. Ogino, K.; Harada, Y.; Kawamura, M.; Hatanaka, K.; Tsuda, S.; Kanai, K.; Katori, M. An inhibitory effect of meloxicam, a novel nonsteroidal anti-inflammatory drug, on COX-2. *Jpn. J. Pharmacol.* **1996**, *71* (Suppl. 2).
20. Świątek, P.; Strzelecka, M.; Urniaz, R.; Gębczak, K.; Gębarowski, T.; Gąsiorowski, K.; Malinka, W. Synthesis, COX-1/2 inhibition activities and molecular docking study of isothiazolopyridine derivatives. *Bioorg. Med. Chem.* **2017**, *25*, 316–326.
21. Ali, M.S.; Al-Lohedan, H.A. Sulfadiazine binds and unfolds bovine serum albumin: An in vitro study. *Mol. Biol. Rep.* **2013**, *40*, 6081–6090. [CrossRef] [PubMed]
22. Chen, G.Z.; Huang, X.Z.; Xu, J.H.; Zheng, Z.Z.; Wang, Z.B. *The Methods of Fluorescence Analysis*, 2nd ed.; Science: Beijing, China, 1990.
23. Lakowicz, J.R. (Ed.) *Principles of Fluorescence Spectroscopy*, 3rd ed.; Springer US: Boston, MA, USA, 2006; ISBN 978-0-387-31278-1.
24. Lakowicz, J.R.; Weber, G. Quenching of fluorescence by oxygen. Probe for structural fluctuations in macromolecules. *Biochemistry* **1973**, *12*, 4161–4170. [CrossRef] [PubMed]
25. Ware, W.R. Oxygen quenching of fluorescence in solution: An experimental study of the diffusion process. *J. Phys. Chem.* **1962**, *66*, 455–458. [CrossRef]
26. Kelly, S.M.; Jess, T.J.; Price, N.C. How to study proteins by circular dichroism. *Biochim. Biophys. Acta Proteins Proteom.* **2005**, *1751*, 119–139. [CrossRef]
27. Kelly, S.M.; Price, N.C. The Use of Circular Dichroism in the Investigation of Protein Structure and Function. *Curr. Protein Pept. Sci.* **2000**, *1*, 349–384. [CrossRef]
28. Lu, Z.X.; Cui, T.; Shi, Q.L. *Applications of Circular Dichroism (CD) and Optical Rotatory Dispersion (ORD) in Molecular Biology*; Science Press: Beijing, China, 1987.
29. Wei, X.L.; Xiao, J.B.; Wang, Y.; Bai, Y. Which model based on fluorescence quenching is suitable to study the interaction between trans-resveratrol and BSA? *Spectrochim. Acta Part. A Mol. Biomol. Spectrosc.* **2010**, *75*, 299–304. [CrossRef]
30. Van De Weert, M.; Stella, L. Fluorescence quenching and ligand binding: A critical discussion of a popular methodology. *J. Mol. Struct.* **2011**, *998*, 145–150. [CrossRef]
31. Bi, S.; Song, D.; Tian, Y.; Zhou, X.; Liu, Z.; Zhang, H. Molecular spectroscopic study on the interaction of tetracyclines with serum albumins. *Spectrochim. Acta Part. A Mol. Biomol. Spectrosc.* **2005**, *61*, 629–636. [CrossRef]
32. Mohammadnia, F.; Fatemi, M.H.; Taghizadeh, S.M. Study on the interaction of anti-inflammatory drugs with human serum albumin using molecular docking, quantitative structure-activity relationship, and fluorescence spectroscopy. *Luminescence* **2020**, *35*, 266–273. [CrossRef]
33. Dufour, C.; Dangles, O. Flavonoid-serum albumin complexation: Determination of binding constants and binding sites by fluorescence spectroscopy. *Biochim. Biophys. Acta Gen. Subj.* **2005**, *1721*, 164–173. [CrossRef] [PubMed]

34. Wani, T.A.; Bakheit, A.H.; Al-Majed, A.R.A.; Bhat, M.A.; Zargar, S. Study of the interactions of bovine serum albumin with the new anti-inflammatory agent 4-(1,3-dsioxo-1,3-dihydro-2H-isoindol-2-yl)-N-[(4-ethoxy-phenyl) methylidene]benzohydrazide using a multi-spectroscopic approach and molecular docking. *Molecules* **2017**, *22*, 1258. [CrossRef] [PubMed]
35. Suryawanshi, V.D.; Walekar, L.S.; Gore, A.H.; Anbhule, P.V.; Kolekar, G.B. Spectroscopic analysis on the binding interaction of biologically active pyrimidine derivative with bovine serum albumin. *J. Pharm. Anal.* **2016**, *6*, 56–63. [CrossRef] [PubMed]
36. Wani, T.A.; Bakheit, A.H.; Zargar, S.; Bhat, M.A.; Al-Majed, A.A. Molecular docking and experimental investigation of new indole derivative cyclooxygenase inhibitor to probe its binding mechanism with bovine serum albumin. *Bioorg. Chem.* **2019**, *89*, 103010. [CrossRef]
37. Abdelhameed, A.S.; Bakheit, A.H.; Mohamed, M.S.; Eldehna, W.M.; Abdel-Aziz, H.A.; Attia, M.I. Synthesis and biophysical insights into the binding of a potent anti-proliferative non-symmetric bis-isatin derivative with bovine serum albumin: Spectroscopic and molecular docking approaches. *Appl. Sci.* **2017**, *7*, 617. [CrossRef]
38. Klotz, I.M.; Urquhart, J.M. The Binding of Organic Ions by Proteins. Effect of Temperature. *J. Am. Chem. Soc.* **1949**, *71*, 847–851. [CrossRef]
39. Ross, P.D.; Subramanian, S. Thermodynamics of protein association reactions: Forces contributing to stability. *Biochemistry* **1981**, *20*, 3096–3102. [CrossRef]
40. Sudlow, G.; Birkett, D.J.; Wade, D.N. The Characterization of two specific drug binding sites on human serum albumin. *Mol. Pharmacol.* **1975**, *11*, 824–832.
41. Sudlow, G.; Birkett, D.J.; Wade, D.N. Further characterization of specific drug binding sites on human serum albumin. *Mol. Pharmacol.* **1976**, *12*, 1052–1061.
42. Becke, A.D. Density-functional thermochemistry. III. The role of exact exchange. *J. Chem. Phys.* **1993**, *98*, 5648. [CrossRef]
43. Lee, C.; Yang, W.; Parr, R.G. Development of the Colle-Salvetti correlation-energy formula into a functional of the electron density. *Phys. Rev. B* **1988**, *37*, 785–789. [CrossRef] [PubMed]
44. Perdew, J.P.; Wang, Y. Accurate and simple analytic representation of the electron-gas correlation energy. *Phys. Rev. B* **1992**, *45*, 13244–13249. [CrossRef] [PubMed]
45. Frisch, M.J.; Trucks, G.W.; Schlegel, H.B.; Scuseria, G.E.; Robb, M.A.; Cheeseman, J.R.; Scalmani, G.; Barone, V.; Petersson, G.A.; Nakatsuji, H.; et al. Gaussian~16 {R}evision {A}.03 2016.
46. Xu, S.; Hermanson, D.J.; Banerjee, S.; Ghebreselasie, K.; Clayton, G.M.; Garavito, R.M.; Marnett, L.J. Oxicams bind in a novel mode to the cyclooxygenase active site via a two-water-mediated h-bonding network. *J. Biol. Chem.* **2014**, *289*, 6799–6808. [CrossRef] [PubMed]
47. Yang, J.M.; Chen, C.C. Gemdock: A generic evolutionary method for molecular docking. *Proteins Struct. Funct. Genet.* **2004**, *55*, 288–304. [CrossRef]
48. Ghuman, J.; Zunszain, P.A.; Petitpas, I.; Bhattacharya, A.A.; Otagiri, M.; Curry, S. Structural basis of the drug-binding specificity of human serum albumin. *J. Mol. Biol.* **2005**, *353*, 38–52. [CrossRef]

Sample Availability: Samples of the compounds A–E. are available from Dominika Szkatuła.